

*Review*

## **Influence of Electrolyte Composition and Voltage on the Microstructure and Growth Mechanism of Plasma Electrolytic Oxidation (PEO) Coatings on Tantalum: A Review**

**Arash Fattah-alhosseini<sup>\*</sup>, Maryam Molaei, and Kazem Babaei**

*Department of Materials Engineering, Bu-Ali Sina University, Hamedan 65178-38695, Iran*

\*Corresponding Author, Tel.: +988138292505; Fax: +988138257400

E-Mail: [a.fattah@basu.ac.ir](mailto:a.fattah@basu.ac.ir)

*Received: 12 March 2020 / Accepted with minor revisions: 12 April 2020 /*

*Published online: 30 April 2020*

---

**Abstract-** Recently, PEO process of tantalum has been developed as a method of producing corrosion-resistant, hard, wear-resistant, and biocompatible as well as having good adhesion coatings. In this review, we present the results of PEO process of tantalum in three main electrolytes. This review tries to measure the effect of electrolyte composition and voltage that were used within PEO procedure on the surface behavior of the produced oxide coatings on Ta. The results of the PEO treatment of Ta in  $H_4SiW_{12}O_{40}$  electrolyte revealed that the morphology of oxide coatings really depends on the PEO procedure time. Density of discharge channels declines as their diameter rises. This leads to an increase in the oxide coating roughness within the PEO procedure of tantalum. In electrolytes of  $\beta$ -glycerophosphate disodium and calcium acetate, the results indicated that the employed voltage significantly affected morphologies, the coatings bond strength and the phase components. However, it affected surface chemical species a little. Finally, in 0.5 M  $Ca(H_2PO_2)_2$  electrolytes, the results revealed that using a precise control on the procedure voltage, tuning the obtained coatings thickness is possible in addition to their roughness, adhesion strength and relative values of the electrolyte type inside the modified surfaces of tantalum.

**Keywords-** Plasma electrolytic oxidation (PEO); Tantalum; Calcium phosphate; 12-tungstosilicic acid;  $\beta$ -glycerophosphate disodium

---

## 1. INTRODUCTION

Having good corrosion resistance and high melting points are the features that have turned the refractory metals as just modern materials that are highly demanded. Tantalum (Ta) is a particular one amongst various refractory metals. In fact, the tantalum use has increased throughout the last two decades. It is logically worth with great qualities like its low temperature of ductile-to-brittle transition, high melting point (2996 °C), biocompatibility, ductility, corrosion resistance, toughness, thermal conductivity strength, wear resistance and so on that has attracted a lot of attention to its splendid capabilities and diverse uses [1]. But, commercially pure tantalum presents several disadvantages. For instance, it shows just an average strength and its high dependency on oxygen results in the production of grain boundary oxides that make embrittlement.

Ta has a high dependency on carbon, nitrogen, hydrogen, oxygen and hydrogen that can create a solid solution containing tantalum. In addition, they are able to react with tantalum in order to make extremely firm compounds like tantalum carbide that raise the tantalum refractory capability [2]. This effect is intensified by a big grain size that was gained after a service with a high-temperature [1]. Ta is totally high-priced and occasionally, it is not definitely economical to fabricate whole pieces of an apparatus using Ta metal. Thus, these appliances are normally made using traditional materials. For instance, stainless steel, and then a tantalum thin solid film is exerted on the surface in order to prepare a corrosion resistant finishing. So, the ultimate product will have Ta properties on its surface whereas keeping the bulk material benefits like cost efficiency and workability of stainless steel within the substrate [2,3].

Corrosion resistance of tantalum depends on a quite firm, dense and non-porous tantalum pentoxide ( $\text{Ta}_2\text{O}_5$ ) film that was formed on its surface while exposing to air or an aqueous ambience. The native  $\text{Ta}_2\text{O}_5$  that is formed on its surface prepares significant protection versus the most corrosive ambience. Although the attendance of distinct metastable phases of Ta-O or suboxides has been recorded properly, the form of pentoxide is the only firm oxide phase at balance that stays in its phase of alpha up to 1320 °C [4]. This oxide layer raises corrosion resistance of tantalum against harmful chemical attacks due to its great stability and adherence [5,6], and functions more efficiently than protective layers that can be formed on Mg, Ti, their alloys and alloys of Co-Cr based in a physiological ambience [7]. Ta other biological qualities such as biocompatibility, hemocompatibility, osseointegration properties, and high radio-opacity have turned it to a perfect alternative for many significant biomedical usages [7,8].

In spite of the fact that Ta presents great passivation tendency inside many aggressive ambiances, it can be easily invaded using hydrofluoric acid at temperatures that are less than 150 °C, free sulfur trioxide and fluoride ions in acidic solution. Moreover, tantalum can be attacked by strong and hot alkalis like boiling aqueous solutions of metal hydroxides but the procedure is slow [2,9,10]. That is due to the fact that Ta is utilized to make procedure

equipment to be used in rough chemical ambiances. Tantalum chemical-mechanical polishing either in alkaline slurries or acid has drawn a lot of attention throughout recent years [2,11].

Stents that are tantalum based are prosperously used in endovascular surgery by presenting significant radio-opacity these days. Therefore, they have been made as a sensible alternative for low-temperature isotropic pyrolytic carbon and converted them into a material options to produce artificial heart valves [12]. Also, porous structures and coatings of tantalum have been discovered to be used in different orthopedic usages like spine surgery, hip and knee arthroplasty, and bone graft substitute by imitating the features of cancellous bone and indicating significant low fatigue strength comparing to generally used biomaterials that are limited in their utility on account of their high density [7,13–15]. As the usage of tantalum having bulk structures is not cost-effective and limited due to its high density, a more sensible choice would be to use coating technologies to create protective coatings of Ta on weaker substrates. This method has been really common these days [7].

## 2. PEO PROCESSING

PEO (occasionally called micro-arc oxidation (MAO)) process that is obtained from common anodic oxidation is an environmental-friendly and effective surface treatment which is mainly exerted on valve metals that are hard to be anodized using usual anodizing processes [16–19]. PEO procedure allows the formation of uniform, thick (typically 10 to 100  $\mu\text{m}$ ) [20] and adherent coatings on metallic pieces with complicated forms [21]. Furthermore, it permits the formation of surfaces having so many diverse natural textures and colors. So, it is really attractive to be used in many usages. PEO industrial usages continues to increase. Also, in the recent years studying it has increased. In addition, commercial and industrial use of this treatment goes on enhancing [22–24].

PEO comes from anodization in which the substrate is located in a bath of an electrolyte and a potential is exerted between an inert cathode and it. According to Fig. 1, PEO process is schematically compared with conventional anodizing procedure. It is evident that this treatment is more complex than usual anodization. Its one reason is that a PEO coating is persistently rebuilt throughout its thickness by the formation of discharge that occurs as growing. Also, there is major scope for controlling the chemical and electrical conditions to modify the coating microstructure [23]. For some metals, especially Al, Ti and Mg, the oxide layer is made on the surface, usually with a very fine, porous and columnar morphology (however other structures are feasible) in addition to a fine-grained and occasionally relatively atomic and amorphous structure [23,25–27].

In PEO process, higher voltages are employed ( $\sim 300\text{--}700\text{ V}$ ), generally connected with an AC electrical supply such that repeated breakdown of dielectric occurs by the growing thickness of oxide layer, such many (micro)-spread discharges that are all over the surface of substrate. In fact, PEO treatment is obtained from DC or AC polarization of a treated specimen

in high potential, making plasma micro-discharges on the surface that tolerates high temperature (up to 4700–6700 °C) in addition to high pressure during its channels. As a result of layers, local effect of high-energy, containing either elements of electrolyte or are formed on the product surface [28]. This mechanism causes the thicker oxide layers formation easier and mainly results in a harder and crystalline microstructure. Generally, as discharges release big values of heat, tending to advance crystallization around oxide material. Indeed, PEO coatings include quite high levels of porosity accompanied by a complex architecture. Nevertheless, they intend to be more wear-resistant than anodized coatings. Furthermore, they are normally able to be increased to a larger thickness [23].

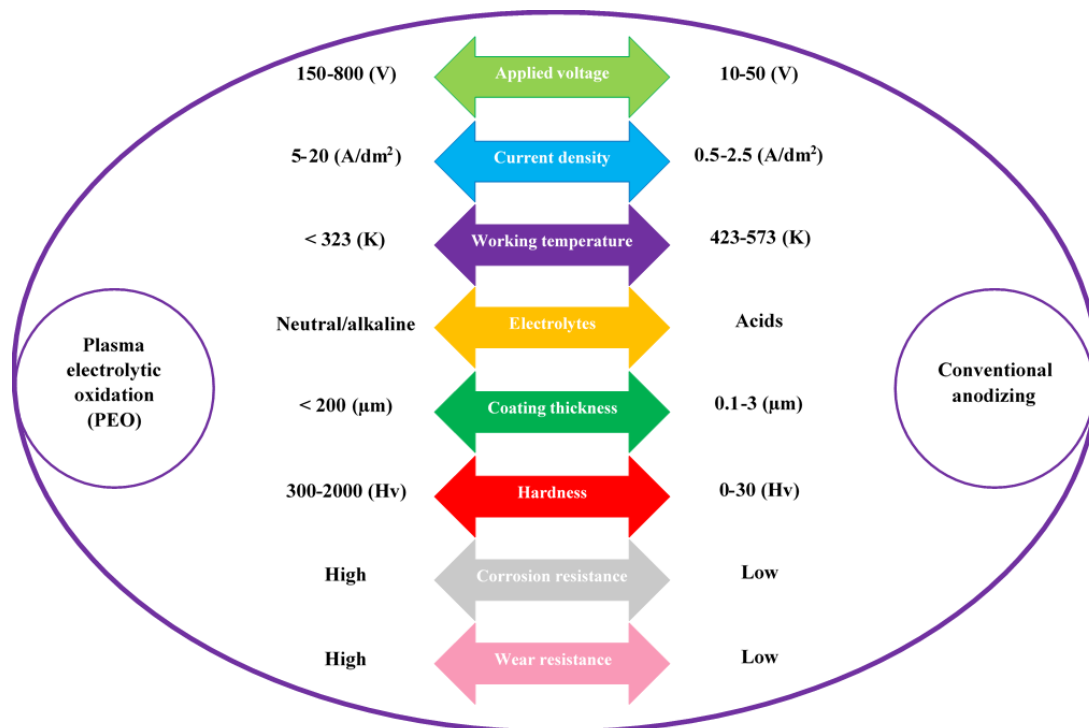


**Fig. 1.** Comparison of PEO process with conventional anodizing process

### 3. METALS USED IN PEO PROCESS

PEO treatment is generally focused on Al and its alloys [29–38], Ti and its alloys [20,39–48], Mg and its alloys [49–57] and Zr and its alloys [58–67]. Fig. 2 shows how the PEO coatings have been applied on different metals and progressed in the last 50 years. The best metals that are oxide coated by PEO in appropriate electrolytes include titanium, aluminum, magnesium, zirconium in addition to their alloys. A lot of authors have reported about PEO procedure and properties of coatings on these metals and their alloys so far. However, few articles about PEO surface treatment on niobium [68–80] and tantalum [81,82,91,92,83–90] have been reported. Table 1 summarizes a list of papers that have studied the chemical compositions and thickness of coatings formed on tantalum.

**Table 1.** Chemical compositions of electrolytes and chemical compositions and thickness of coating

Electrolytes	PEO treatment condition	Phase compositions of coatings	Coating thickness (μm)	Year	First author [Ref]
0.001 M H <sub>4</sub> SiW <sub>12</sub> O <sub>40</sub> (pH: 2.8 and T: 21 ± 1 °C)	70 mA/cm <sup>2</sup>	---	---	2011	[81] Stojadinović
(pH: 2.8 and T: 21 ± 1 °C) 0.001 M H <sub>4</sub> SiW <sub>12</sub> O <sub>40</sub>	70 mA/cm <sup>2</sup>	WO <sub>3</sub> , Ta <sub>2</sub> O <sub>5</sub> , SiO <sub>2</sub>	---	2011	[82] Petkovic
0.1, 0.5 and 1 mol/dm <sup>3</sup> K <sub>2</sub> SiO <sub>3</sub> + 5 g/dm <sup>3</sup> KOH	Current density: 0.1 A/dm <sup>2</sup> (up to a voltages of 100, 200 or 400 V) Treatment time: 5 min	Ta <sub>2</sub> O <sub>5</sub>	0.56-8.69	2013	[83] Sowa
β-glycerophosphate disodium (T: 20 °C) 0.2 M calcium acetate + 0.02 M	Positive pulse voltage: 450 V Negative pulse voltage: 70 V Pulse frequency: 100 Hz Duty ratio: 26% Treatment time: 1-20 min	CaTa <sub>2</sub> O <sub>6</sub> Ta <sub>2</sub> O <sub>5</sub> TaO	1.2 and 1.7	2013	[84] Wang
<b>A:</b> 5 g/l Na <sub>2</sub> SiO <sub>3</sub> ·5H <sub>2</sub> O + 1 g/l KOH (T: not exceed 30 °C) <b>B:</b> 5 g/l Na <sub>3</sub> PO <sub>4</sub> + 1 g/l KOH (T: not exceed 30 °C)	Current density: 0.085 A/cm <sup>2</sup> Treatment time: 30 min	Tantalum oxide Sodium tantalates	---	2014	[85] Gao
300 g Cu(NO <sub>3</sub> ) <sub>2</sub> + 300 g Ca(NO <sub>3</sub> ) <sub>2</sub> in 1 l of H <sub>3</sub> PO <sub>4</sub> (85%) (T: 20±2 °C)	DC voltage: 450 ± 10V Treatment time: 3 min	Tantalum phosphate	---	2016	[86] Rokosz
0.2 M calcium acetate + 0.02 M β-glycerophosphate disodium	Treatment time: 1, 3 and 5 min	---	---	2016	[87] Goularte
0.2 M calcium acetate + 0.02 M β-glycerophosphate disodium (T: 20 °C)	Pulse voltages: 350, 400, 450 and 480 V Negative pulse voltage: 70 V Pulse frequency: 100 Hz Duty ratio: 26% Treatment time: 10 min	Ta <sub>2</sub> O <sub>5</sub> CaTa <sub>2</sub> O <sub>6</sub> TaO	5-20	2016	[88] Wang
0.2 M calcium acetate + 0.02 M β-glycerophosphate disodium (T < 30 °C)	Frequency: 100 Hz Duty ratio: 40%	CaTa <sub>2</sub> O <sub>6</sub> , Ta <sub>2</sub> O <sub>5</sub> , TaO	---	2017	[89] Zhao
<b>A:</b> 0.5 M Ca(H <sub>2</sub> PO <sub>2</sub> ) <sub>2</sub> <b>B:</b> 0.5 M Ca(H <sub>2</sub> PO <sub>2</sub> ) <sub>2</sub> + 1.15 M Ca(HCOO) <sub>2</sub> <b>C:</b> 0.5 M Ca(H <sub>2</sub> PO <sub>2</sub> ) <sub>2</sub> + 1.15 M Mg(CH <sub>3</sub> COO) <sub>2</sub> <b>D:</b> 0.5 M Ca(H <sub>2</sub> PO <sub>2</sub> ) <sub>2</sub> + 1.50 M Mg(CH <sub>3</sub> COO) <sub>2</sub>	Current density: 150 mA/cm <sup>2</sup> (up to the desired limiting voltages of 200, 300, 400 and 500 V)	Ca(PO <sub>3</sub> ) <sub>2</sub> ·2H <sub>2</sub> O MgCO <sub>3</sub> Ca <sub>2</sub> P <sub>2</sub> O <sub>7</sub> Ca <sub>4</sub> Mg <sub>5</sub> (PO <sub>4</sub> ) <sub>6</sub> Ca <sub>3</sub> (PO <sub>4</sub> ) <sub>2</sub> Ca <sub>5</sub> (PO <sub>4</sub> ) <sub>3</sub> (OH) CaTa <sub>2</sub> O <sub>6</sub>	1.48-144	2017	[90] Sowa
<b>A:</b> 0.5 M Ca(H <sub>2</sub> PO <sub>2</sub> ) <sub>2</sub> <b>B:</b> 0.5 M Ca(H <sub>2</sub> PO <sub>2</sub> ) <sub>2</sub> + 1.15 M Ca(HCOO) <sub>2</sub> <b>C:</b> 0.5 M Ca(H <sub>2</sub> PO <sub>2</sub> ) <sub>2</sub> + 1.15 M Mg(HCOO) <sub>2</sub>	Current density: 150 mA/cm <sup>2</sup> (up to one of the three limiting voltages of 200, 300 or 400 V) Treatment time: 5 min	CaTa <sub>2</sub> O <sub>6</sub>	~1-65	2018	[91] Sowa
β-glycerophosphate disodium (T: 25-60 °C) 0.2 M calcium acetate + 0.02 M	Pulses: 350, 450 and 500 V at repetition rate of 100 Hz Duty ratio: 60% Treatment time: 1-10 min	Ta <sub>2</sub> O <sub>5</sub> CaTa <sub>2</sub> O <sub>6</sub> Ca <sub>3</sub> (PO <sub>4</sub> ) <sub>2</sub> Hydroxyapatite	~19-43	2019	[92] Antonio

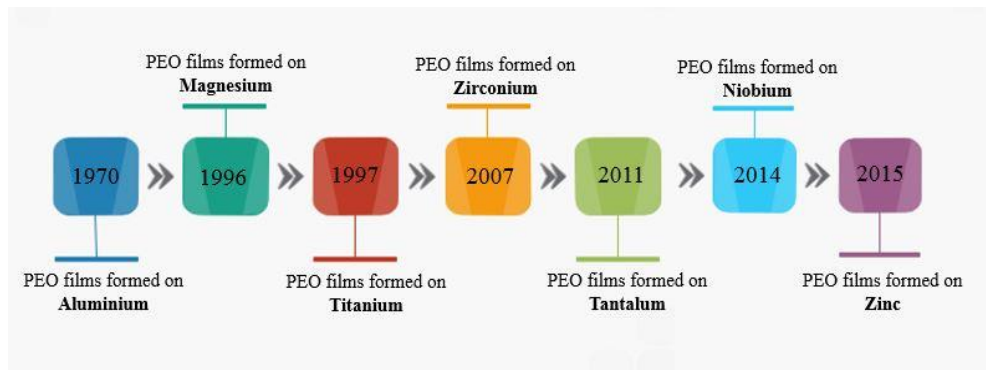


**Fig. 2.** PEO coatings schematic improvements of different metals in the last decades

Tantalum is mostly a very fascinating coating material because of its capability of growing stable oxides having good properties of dielectric, high melting point, hardness, good thermal conductivity, good resistance against wear and temperature [82]. The present review concentrates on PEO coatings that have been applied on tantalum. That is because of the growth of stable oxide films on Ta using PEO procedure that can improve their mechanical behaviors that is really significant in different applications [82].

All curves of voltage–time indicated three stages (Fig. 3) in PEO process. At beginning of the PEO treatment called “stage 1”, potential increased linearly and quickly while the time passing due to the formation of a thin barrier layer on the surface (anode).

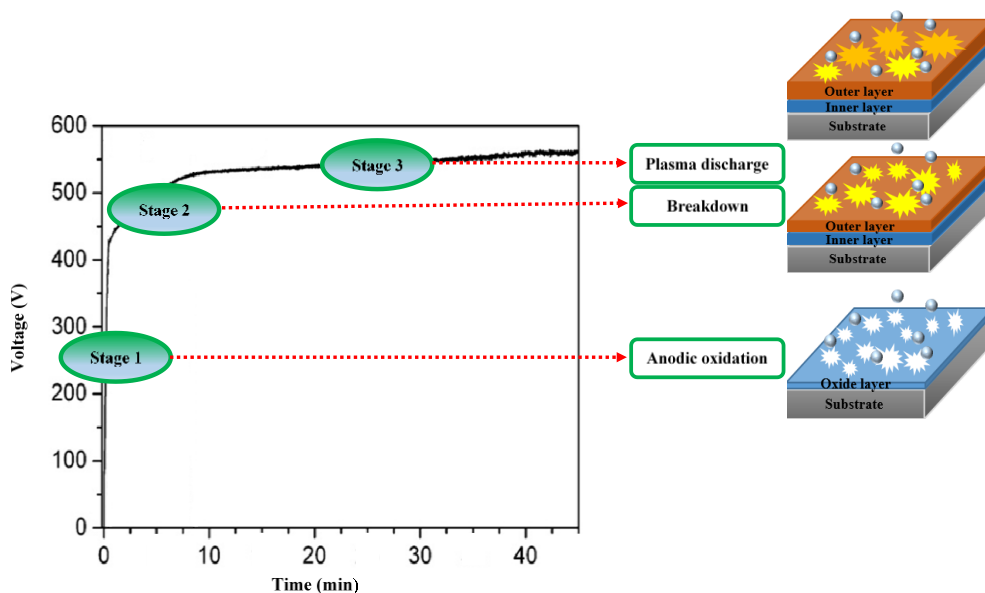


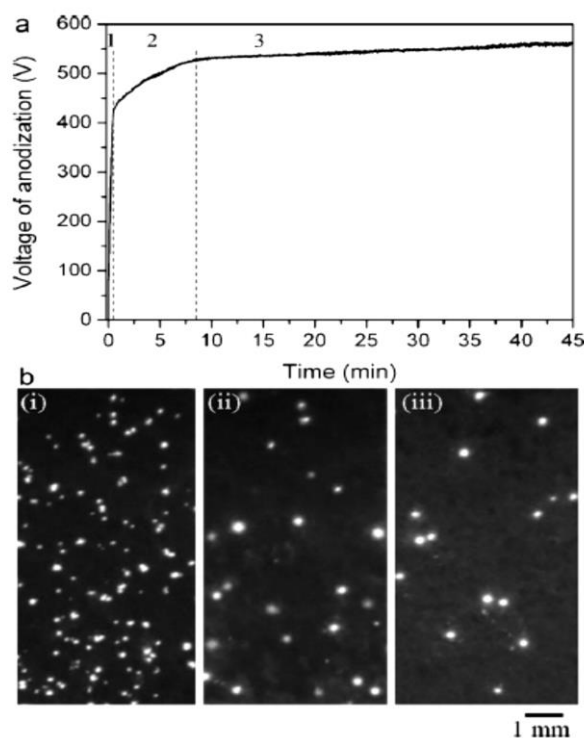
**Fig. 3.** Schematic of the cell potential-time and formation process of PEO coating

In the second stage, the potential increased with time in a lower ratio in comparison to stage 1 and then the weak parts breakdown of the oxide film occurred. After increasing the breakdown potential, many small and white transient sparks that were specified by the concentration and composition of the electrolyte and metal were appeared on the surface and

the potential increased slightly. In this step, the growth rate of coating decreased on account of the coating growth and dissolution. Potential reached a really constant value and sparks got keener in the third stage called “the micro-arc step”. The color of sparks also shifted to yellow and then after that turned into orange slightly [37,93].

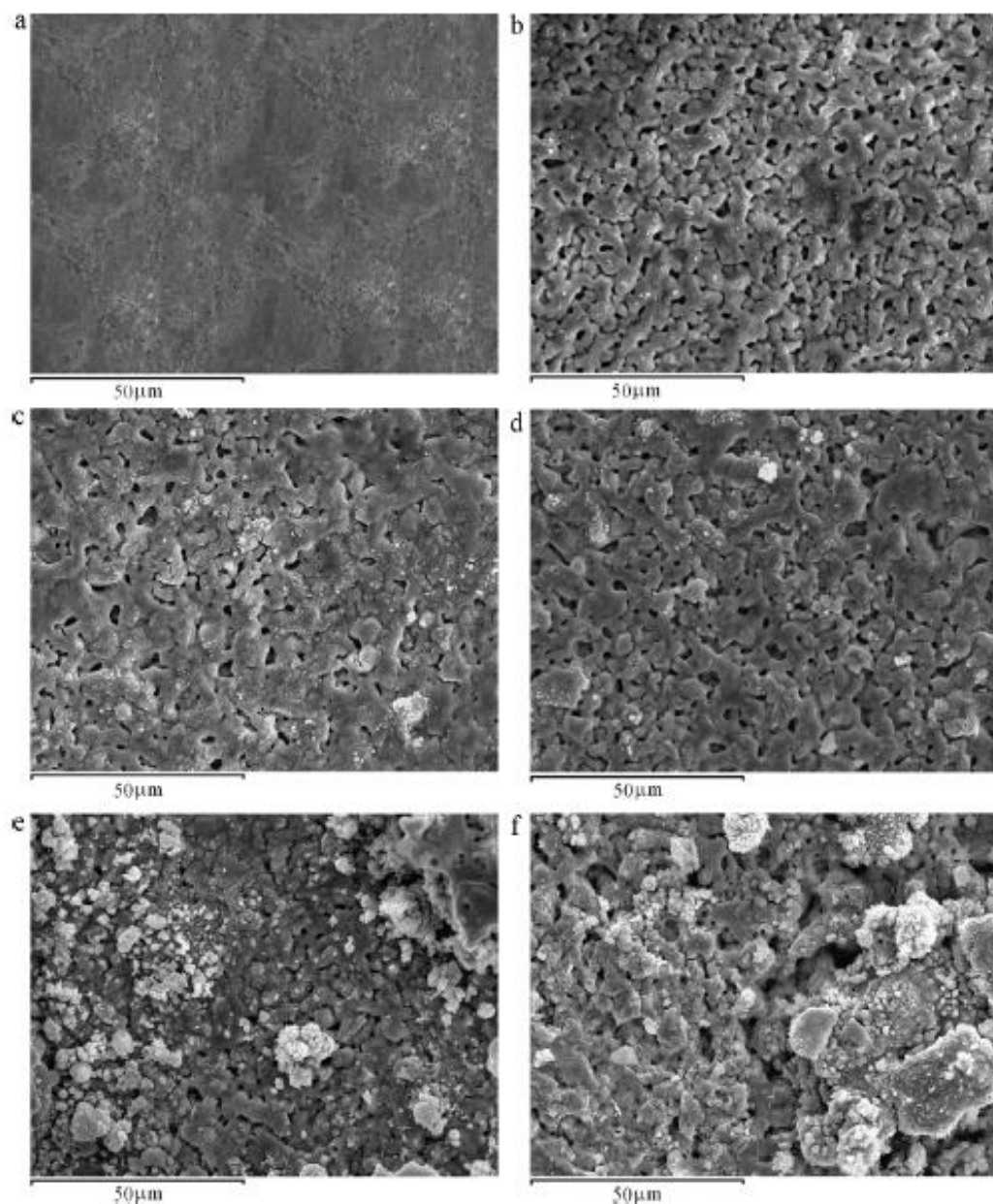
#### 4. PEO TREATMENT OF Ta IN 12-TUNGSTOSILICIC ACID

Fig. 4(a) indicates voltage–time response within tantalum PEO treatment in 12-tungstosilicic acid of 0.001 M [82]. The voltage augments almost linearly with time to around 420 V in a little time leading to the fixed rate of an increase in the oxide layer thickness from the start of anodization. This step is followed by obvious deviation from linearity of voltage–time plot, beginning from breakdown (sparking) voltage. Fig. 4(a) shows that voltage increases constantly. However, the slope of voltage–time declines and many small size micro-discharges become visible, equally spread over the whole surface of specimen after the breakdown. More anodization leads to fairly constant value of the anodization voltage. The micro-discharges size get bigger when micro-discharges spatial density gets less while increasing PEO procedure time (Fig. 4(b)) [82].



**Fig. 4.** (a) Voltage vs. time relationship recorded during PEO of Ta in 0.001 M  $\text{H}_4\text{SiW}_{12}\text{O}_{40}$  at  $70 \text{ mA/cm}^2$ ; (b) Micro-discharges appearance at various steps of the PEO treatment: (i) 120 s; (ii) 600 s; (iii) 2400 s [82]. (With permission from Ref. [82]; License Number: 4775700463627, Feb 24, 2020).

The PEO procedure can be separated into three steps according to the voltage–time plot. In the first step, the strength of electric field for a certain current density remains stable within the anodic growth and the ionic current is two to three orders of magnitude larger than that of the electronic part. The anodization voltage should have a linear increase while the thickness of film to keep the strength of electric field in a constant status. Moreover, the electric field producing avalanches injects electrons and accelerates them into the conduction band of the anodic oxide using a mechanism impact ionization within anodization.



**Fig. 5.** SEM images of the PEO coatings formed on Ta in 0.001 M H<sub>4</sub>SiW<sub>12</sub>O<sub>40</sub> at various steps of PEO treatment: (a) 15 s; (b) 180 s; (c) 600 s; (d) 900 s; (e) 1800 s; (f) 2700 s [82]. (With permission from Ref. [82]; License Number: 4775700463627, Feb 24, 2020).

The breakdown occurs as the current of avalanche electronic gets critical value. In the second step, a fairly low voltage is needed to keep the similar overall current density, because of the electron current density independence having thickness of anodic oxide layer. In the third step, the fraction of electron current density in overall current density gets dominant. The total current density is independent from thickness of anodic oxide layer. Furthermore, the voltage–time slope is near zero in this step [81,82].

Micrographs of SEM for the oxide surface are indicated in Fig. 5 before and after breakdown [82]. The fairly compact oxide layers are created before breakdown (Fig. 5(a)). Then after breakdown the surface of oxide gets laced with some micro-discharge channels in addition to molten areas created because of quick cooling influence of the electrolyte (Fig. 5(b)–(f)). The oxide layers breakdown is operated using effects of local heating that were arisen from highly localized procedures occurring at macro and micro-defects inside the oxide. In a thicker film of oxide coating, the current needs higher energy go through the coating. In this status, the current is localized at weak points of the formed film in order to find its mechanism through the coating. As a result, the discharge channel diameter will rise. In addition, the thicker the coatings are, the higher surface roughness is [81,82].

## 5. PEO TREATMENT OF Ta IN CALCIUM ACETATE AND $\beta$ -GLYCEROPHOSPHATE DISODIUM SOLUTIONS

Wang et al. [84] indicated the Ta PEO coatings XRD patterns in calcium acetate and  $\beta$ -glycerophosphate disodium solutions at 450 V for 60, 180, 300, 600 and 900 s (Fig. 6).

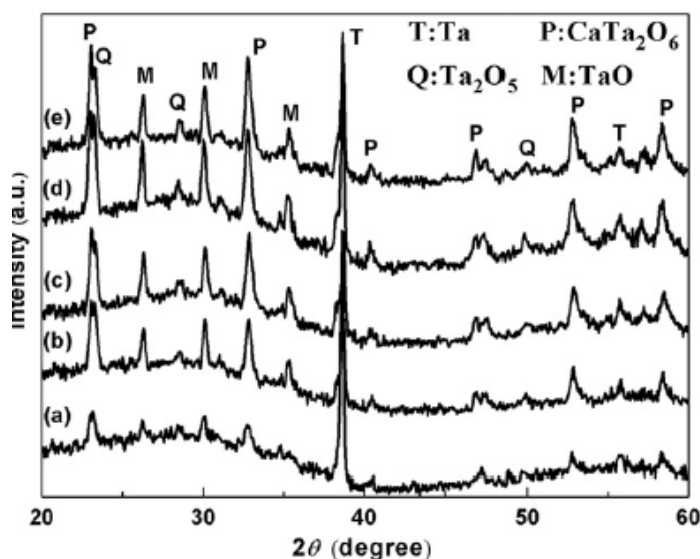


**Fig. 6.** XRD spectra of oxide coatings formed on Ta in calcium acetate and  $\beta$ -glycerophosphate disodium solutions at 450 V for (a) 60 s, (b) 180 s, (c) 300 s, (d) 600 s and (e) 900 s [84]. (With permission from Ref. [84]; License Number: 4775700767355, Feb 24, 2020).

These XRD patterns exhibited that the coatings consist of  $\text{CaTa}_2\text{O}_6$ ,  $\text{Ta}_2\text{O}_5$  and  $\text{TaO}$  phases in which  $\text{CaTa}_2\text{O}_6$  is the dominant component. It is also proved that the intensities of the phase diffraction peaks increase. However, no new phases is produced by rising the MAO time, showing that the MAO time is not able to modify the coatings phases in the applied voltage [84]. In the other paper, Wang et al. [88] explained the PEO coatings XRD patterns that were formed at 350 V, 400 V, 450 V and 480 V for 600 s (Fig. 7). The peaks of Ta are ascribed to the contribution from the Ta substrate and the broadened spectra located at  $20\text{--}35^\circ$  depict that there is an amorphous phase within the PEO coatings. As can be observed in Fig. 7, the PEO coating that was formed at 350 V is mostly composed of the amorphous phase and shows extra  $\text{Ta}_2\text{O}_5$  diffraction peaks. Also,  $\text{TaO}$  and  $\text{CaTa}_2\text{O}_6$  spectra are discovered in the coatings that were formed at the employed potential which was higher than 350 V and feel like to augment by rising the potential as the broadened peaks located at  $20\text{--}35^\circ$  get weaker that shows the amount of the amorphous phase slightly declines. For 480 V, the formed PEO coating on tantalum are com-posed of  $\text{Ta}_2\text{O}_5$ ,  $\text{TaO}$ ,  $\text{CaTa}_2\text{O}_6$  and a bit amorphous phase inside the outer areas of the layer in which  $\text{CaTa}_2\text{O}_6$  is the dominant component [88]. Zhao et al. [89] discovered the similar XRD patterns of Ta PEO coatings in  $\beta$ -glycerophosphate disodium and calcium acetate solutions.

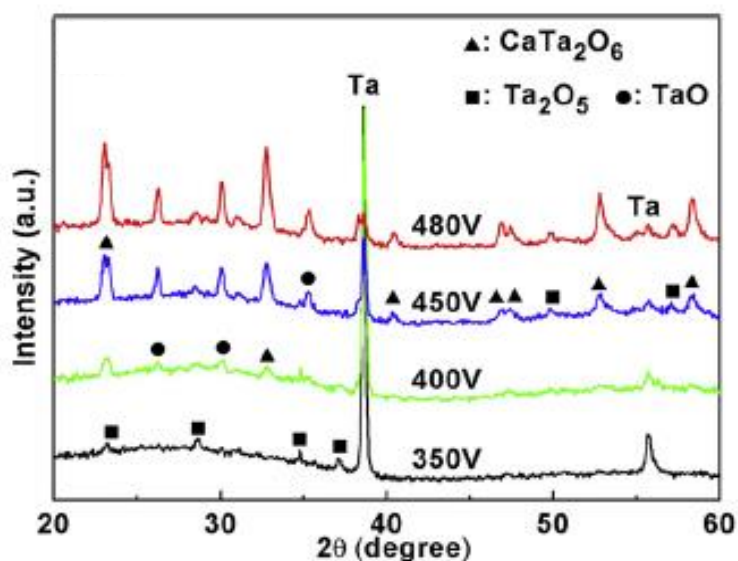


**Fig. 7.** XRD patterns of oxide coatings formed on Ta in calcium acetate and  $\beta$ -glycerophosphate disodium solutions at 350, 400, 450 and 480 V [88]. (With permission from Ref. [88]; License Number: 4775700988566, Feb 24, 2020).

## 6. PEO TREATMENT OF Ta IN 0.5 M $\text{Ca}(\text{H}_2\text{PO}_2)_2$ SOLUTIONS

Sowa et al. [90] studied the influence of applied voltage and composition of electrolyte that were utilized within PEO on the surface behaviors for the resulting oxide coatings on Ta. The

PEO treatment was discovered in 0.50 M  $\text{Ca}(\text{H}_2\text{PO}_2)_2$  solution that was modified using the addition of 1.15 M  $\text{Ca}(\text{HCOO})_2$  in addition to 1.15 and 1.50 M  $\text{Mg}(\text{CH}_3\text{COO})_2$ . Current and voltage altered with time and were recorded throughout the PEO process of tantalum samples and the plots are illustrated in Fig. 8 [90]. For electrolyte of A as can be seen in Fig. 8(a), the voltage was precisely rising with time within the beginning seconds of the procedure. Thus, there was a slight decline in the slope of voltage-time that was related to the appearance of the first sparks throughout the anodization. The sparks were the results of the oxide layer or/and oxygen gas dielectric breakdown. After the transient area between  $\sim 150$  and  $\sim 250$  V, another area could be recognized that had an increase in the linear voltage and it was seen up to 300 V. there was still another area in which little perturbations of voltage versus time could be considered between 300 and 400 V. The perturbations depended on the beginning of stronger sparks that were fewer and keener. After achieving  $\sim 400$  V, the perturbations were slightly rising in amplitude during the whole procedure time.

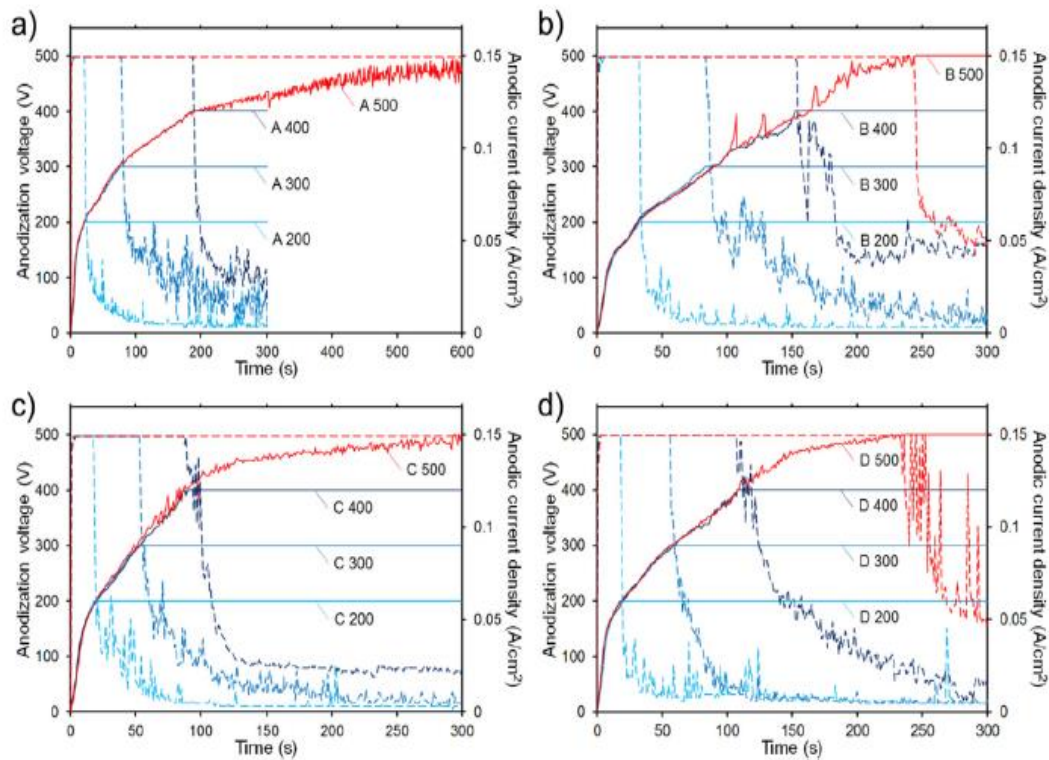


**Fig. 8.** Voltage and current vs. treatment time during PEO process of Ta in 0.5 M  $\text{Ca}(\text{H}_2\text{PO}_2)_2$  electrolytes (A, B, C and D (see table 1)) [90]. (With permission from Ref. [90]; License Number: 4775701188039, Feb 24, 2020).

After adding the second element (calcium formate) to the main electrolyte, the developments in current time and voltage were considerably changed comparing with those for the solution of A as can be seen in Fig. 8(b). Voltage oscillations related to strong sparks were seen after applying 300 V till the first stage of the procedure. Except for the first area where

the increase in voltage rate was more gradual comparing with the solution of A, all the slopes were steeper in the case for electrolyte of B. This electrolyte also had a lower breakdown voltage. The increase in solution conductivity was the reason of these observations that influenced the voltage drop through the oxide film within the process. The more charge carriers within the electrolyte, the less resistive the solution was and a great part of applied voltage drop was ascribed to the electrochemical interface. Moreover, the start of the bigger sparks was considered lower, that is in a good agreement with the discussion above. For the solution C as shown in Fig. 8(c), the developments in voltage and current time were totally distinct from the former two ones. Three linear areas could be recognized. Although ~300 s was sufficient to reach the restricting potential of ~500 V, the second stage in the anodization did not occur due to the limitation of time. For the solution D as shown in Fig. 8(d), the curve of progression was same as that for the solution of C. Then after the first linear area, another quasi-linear area could be recognized that was followed by a really smooth and turbulent rise in the applied voltage to the final restricting voltage. Compared to the obtained results from Sowa et al. [83], the increase in voltage was much lower for the phosphate-based electrolyte versus solutions of silicate based and the plots possessed fewer features. In addition, Petković et al. [82] have realized three voltage vs. time relationships within the PEO process. In the first area, the voltage sharp linear increase was attributed to the anodization procedure having the anodic reactions [90]:



This procedure results in thickening the oxide film that is required to keep the constant electric field throughout the oxide film [90].

## 7. COMPARING THE PEO COATING FORMATION MECHANISM IN VALVE METALS AND Ta

PEO treatment has been highly applied on valve metals like an effective way to modify the surface and has been approved to lead to a major improvement on these alloys corrosion resistance [94,95]. Fig. 9 presents the schematic of the structural characteristics for PEO coating that was formed in low voltages (Voltages < breakdown potential) and high voltages (Voltages > breakdown potential) on tantalum and also valve metals. A double-layer structure is composed of an inner compact layer and an outer porous layer was formed in PEO process in terms of valve metals [96,97]. Generally, the generation of PEO coating on valve metals is halved into totally different stages [94,98,99]: (i) a barrier layer (dense and thin oxide layer) is formed on the surface under a quite low anodic voltage (Fig. 9(a)). There is no spark in this step. (ii) When the voltage rises the breakdown voltage threshold, the loss of dielectric stability results in the generation of discharge channels in the low dielectric zone [94,98,99]. Thus,

several micro-sparks are generated in the thinner or weaker spots and move rapidly through the oxide layer. Although any spark lifetime is no longer than 1 ms, the local temperature at the discharge channels can make molten substrate and anodic film be generated [99,100].

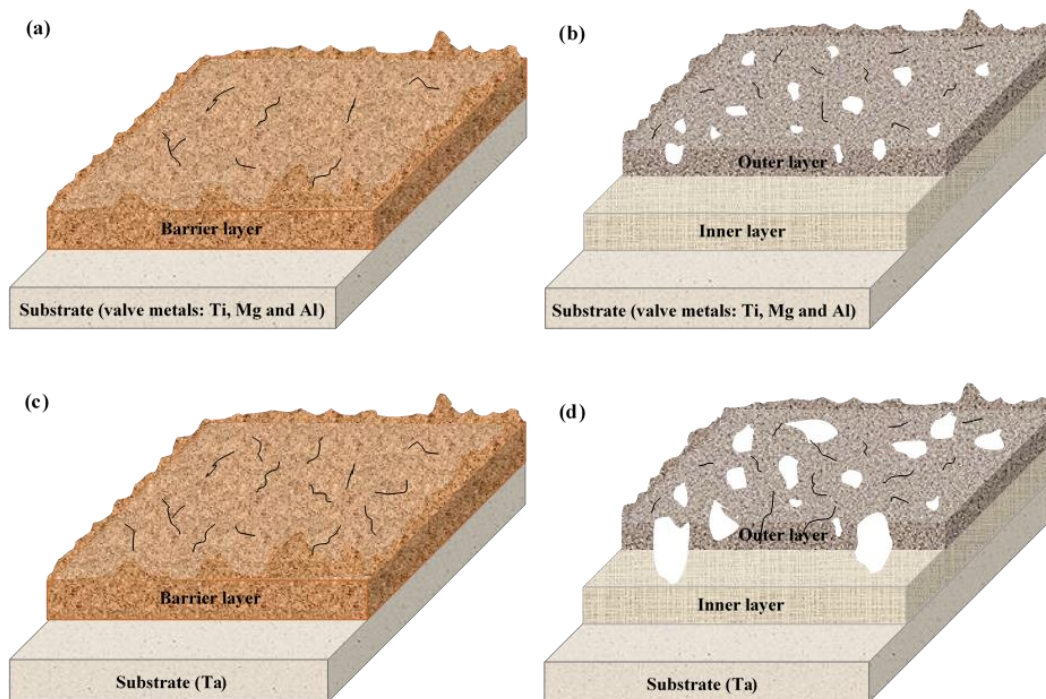


**Fig. 9.** Schematic of the structural characteristics of PEO coating formed in low and high potential on (a, b) valve metals and (c, d) Ta.

A little of melt is in discharge channel and the products are formed on the discharge channels walls while is cooled by solution. Thus, thickness rises and porous structure is revealed as Fig. 9(b). In the growth of PEO coating, the compact inner layer comes into the initial stage of discharge sparking as the voltage surpassing the breakdown potential [101]. The generation of PEO coating on tantalum shows a comparable process comparing with valve metals. A thin anodic film is produced at the stage 1. Consequently, a thick and porous coating is formed as the voltage increases through the voltage of breakdown. However, the compact inner layer is destroyed in terms of PEO process on tantalum (Fig. 9(d)). It is discovered that in the stage 1 and before the spark anodization, a barrier layer can be produced over the surface in terms of valve metals while, these dense and passive oxide layers do not exist in terms of non-valve metals such as Ta, Zn, Fe, etc [94,102,103]. Overall, the anodic film which was formed in low voltage is removed with a lot of pores and cracks shared through the cross-section as presented in Fig. 9(c). Therefore, it is assumed these defects were produced in low voltage in the anodic layer resulting in the incoherent compact inner structure under the condition of high gas release and micro-arcs in the beginning sparking discharge stage [94].

## 8. CONCLUSIONS

The results of PEO process of tantalum in three main electrolytes were presented as below:

1. Tantalum PEO procedure in  $\text{H}_4\text{SiW}_{12}\text{O}_{40}$  is distributed to three different stages based on the changes in the response of voltage-time. The electron current density portion in whole current density within the anodization leads to the transformation of voltage-time curve slope. The morphology of oxide coatings highly depends on the time in PEO procedure. Discharge channels density declines as their diameter rises, leading to an increase in the oxide coating roughness during the PEO treatment of Ta. The primary elements in PEO coatings include O, Ta, Si and W. The coatings are slightly crystallized and mostly contain  $\text{Ta}_2\text{O}_5$ ,  $\text{SiO}_2$  and  $\text{WO}_3$ .

2. The results of the PEO process of Ta in electrolytes of  $\beta$ -glycerophosphate disodium and calcium acetate showed that the employed voltage significantly had an effect on the morphologies phase elements and the coatings bond strength. However, it slightly affected surface chemical species. The PEO oxide coating was formed at 350 V mostly composed of an amorphous phase and indicates extra  $\text{Ta}_2\text{O}_5$  diffraction peaks and by rising the employed voltage to 480 V, the produced PEO coatings on tantalum consisted of  $\text{Ta}_2\text{O}_5$ ,  $\text{CaTa}_2\text{O}_6$  and TaO in addition to a bit amorphous phase in which  $\text{CaTa}_2\text{O}_6$  was a dominant element. While rising the employed voltage, the diameter of the pores aimed to augment as the number of the pores declined and the coatings bond strength declined.

3. The results of the of tantalum PEO treatment in solutions of 0.5 M  $\text{Ca}(\text{H}_2\text{PO}_2)_2$  demonstrated that it is possible to tune the obtained coatings thickness in addition to their roughness, adhesion strength and comparative amounts of the different types of electrolytes in the modified surfaces of tantalum by a precise control on the voltage of process. Moreover, the results indicated that by adding salts of  $\text{Ca}^{2+}$  and  $\text{Mg}^{2+}$  carboxylic, that were mainly utilized by recent researchers within PEO procedure and leads to the sparks intensification on the surfaces that were treated.

## REFERENCES

- [1] M. Bischof, S. Mayer, H. Leitner, H. Clemens, P. Staron, E. Geiger, A. Voiticek, and W. Knabl, *Int. J. Refract. Met. Hard Mater.* 24 (2006) 437.
- [2] A. Fattah-alhosseini, F.R. Attarzadeh, S. Vafaeian, M. Haghshenas, and M.K. Keshavarz, *Int. J. Refract. Met. Hard Mater.* 64 (2017) 168.
- [3] A. Fattah-alhosseini, and S.T. Shojae, *Mater. Res. Express.* 5 (2018) 116512.
- [4] M. Khanuja, H. Sharma, B.R. Mehta, and S.M. Shivaprasad, *J. Electron Spectros. Relat. Phenomena.* 169 (2009) 41.
- [5] F.R. Attarzadeh, N. Attarzadeh, S. Vafaeian, and A. Fattah-alhosseini, *J. Mater. Eng. Perform.* 25 (2016) 4199.
- [6] A. Fattah-alhosseini, and S. Sharifi, *Anal. Bioanal. Electrochem.* 9 (2017) 862.
- [7] A. Fattah-alhosseini, H. Elmkhah, G. Ansari, F. Attarzadeh, and O. Imantalab, *J. Alloys*

- Compd. 739 (2018) 918.
- [8] H. Matsuno, A. Yokoyama, F. Watari, M. Uo, and T. Kawasaki, *Biomaterials*. 22 (2001) 1253.
- [9] S.M. Cardonne, P. Kumar, C.A. Michaluk, and H.D. Schwartz, *Int. J. Refract. Met. Hard Mater.* 13 (1995) 187.
- [10] A. Fattah-alhosseini, S. Vafaeian, A.R. Ansari, and M. Khanmohammadi, *Anal. Bioanal. Electrochem.* 9 (2017) 660.
- [11] A. Robin, and J.L. Rosa, *Int. J. Refract. Met. Hard Mater.* 18 (2000) 13.
- [12] A. Fattah-alhosseini, H. Elmkhah, K. Babaei, O. Imantalab, H.R. Ghomi, and M.K. Keshavarz, *Mater. Res. Express.* 5 (2018) 106401.
- [13] A.F. Kamath, G.C. Lee, N.P. Sheth, C.L. Nelson, J.P. Garino, and C.L. Israelite, *J. Arthroplasty*. 26 (2011) 1390.
- [14] A. Fattah-alhosseini, and M. Pourmahmoud, *J. Mater. Eng. Perform.* 27 (2018) 116.
- [15] Q. Chen, and G.A. Thouas, *Mater. Sci. Eng. R.* 87 (2015) 1.
- [16] R.O. Hussein, X. Nie, D.O. Northwood, A. Yerokhin, and A. Matthews, *J. Phys. D. Appl. Phys.* 43 (2010) 105203.
- [17] F.C. Walsh, C.T.J. Low, R.J.K. Wood, K.T. Stevens, J. Archer, A.R. Poeton, and A. Ryder, *Trans. Inst. Met. Finish.* 87 (2009) 122.
- [18] A. Fattah-alhosseini, M.K. Keshavarz, M. Molaei, and S.O. Gashti, *Metall. Mater. Trans. A.* 49 (2018) 4966.
- [19] M. Sabaghi Joni, and A. Fattah-alhosseini, *J. Alloys Compd.* 661 (2016) 237.
- [20] M. Molaei, A. Fattah-alhosseini, and S.O. Gashti, *Metall. Mater. Trans. A* 49 (2018) 368.
- [21] X. Lu, M. Mohedano, C. Blawert, E. Matykina, R. Arrabal, K.U. Kainer, and M.L. Zheludkevich, *Surf. Coatings Technol.* 307 (2016) 1165.
- [22] A.L.L. Yerokhin, X. Nie, A. Leyland, A. Matthews, and S.J.J. Dowey, *Surf. Coatings Technol.* 122 (1999) 73.
- [23] T.W. Clyne, and S.C. Troughton, *Int. Mater. Rev.* 64 (2019) 127.
- [24] R.O. Hussein, X. Nie, and D.O. Northwood, *Electrochim. Acta.* 112 (2013) 111.
- [25] P. Skeldon, G.E. Thompson, and G.C. Wood, *Thin Solid Films.* 148 (1987) 333.
- [26] R.O. Mota, Y. Liu, O.R. Mattos, P. Skeldon, and G.E. Thompson, *Corros. Sci.* 50 (2008) 1391.
- [27] M. Vakili-Azghandi, A. Fattah-alhosseini, and M.K. Keshavarz, *Meas. J. Int. Meas. Confed.* 124 (2018) 252.
- [28] S.V. Gnedenkov, Y.P. Sharkeev, S.L. Sinebryukhov, O.A. Khrisanfova, E.V. Legostaeva, A.G. Zavidnaya, A.V. Puz', I.A. Khlusov, and D.P. Opra, *Corros. Rev.* 34 (2016) 65.
- [29] A.L. Yerokhin, L.O. Snizhko, N.L. Gurevina, A. Leyland, A. Pilkington, and A.

- Matthews, J. *Phys. D Appl. Phys.* 36 (2003) 2110.
- [30] B. Wielage, G. Alisch, T. Lampke, and D. Nickel, *Key Eng. Mater.* 384 (2008) 263.
- [31] A. Fattah-alhosseini, M. Vakili-Azghandi, and M.K. Keshavarz, *Acta Metall. Sin. (English Lett.)* 29 (2016) 274.
- [32] V.K. Patel, and S. Bhowmik, *Rev. Adhes. Adhes.* 5 (2017) 79.
- [33] Z. Masoomi Loghman, A. Fattah-alhosseini, and S.O. Gashti, *Anal. Bioanal. Electrochem.* 10 (2018) 1247.
- [34] M. Vakili-Azghandi, and A. Fattah-alhosseini, *Metall. Mater. Trans. A.* 48 (2017) 4681.
- [35] M. Vakili-Azghandi, A. Fattah-alhosseini, and M.K. Keshavarz, *J. Mater. Eng. Perform.* 25 (2016) 5302.
- [36] Z. Masoomi Loghman, A. Fattah-alhosseini, and S.O. Gashti, *Anal. Bioanal. Electrochem.* 11 (2019) 1020.
- [37] A. Fattah-alhosseini, S.O. Gashti, and M. Molaie, *J. Mater. Eng. Perform.* 27 (2018) 825.
- [38] A. Khodabandeloie, and A. Fattah-alhosseini, *Anal. Bioanal. Electrochem.* 10 (2018) 1574.
- [39] A.R.R. Rafieerad, M.R.R. Ashra, R. Mahmoodian, and A.R.R. Bushroa, *Mater. Sci. Eng. C.* 57 (2015) 397.
- [40] E. Nikoomanzari, A. Fattah-alhosseini, M.R. Pajohi Alamoti, and M.K. Keshavarz, *Ceram. Int.* <https://doi.org/10.1016/j.ceramint.2020.02.084>.
- [41] M. Molaei, A. Fattah-alhosseini, and M.K. Keshavarz, *J. Asian Ceram. Soc.* 7 (2019) 247.
- [42] A. Krzakała, A. Kazek-Kęsik, and W. Simka, *RSC Adv.* 3 (2013) 19725.
- [43] M. Roknian, A. Fattah-alhosseini, and S.O. Gashti, *J. Mater. Eng. Perform.* 27 (2018) 1343.
- [44] A. Lugovskoy, and S. Lugovskoy, *Mater. Sci. Eng. C.* 43 (2014) 527.
- [45] M. Roknian, A. Fattah-alhosseini, S.O. Gashti, and M.K. Keshavarz, *J. Alloys Compd.* 740 (2018) 330.
- [46] Y. Wang, H. Yu, C. Chen, and Z. Zhao, *Mater. Des.* 85 (2015) 640.
- [47] A. Gao, R. Hang, L. Bai, B. Tang, and P.K. Chu, *Electrochim. Acta.* 271 (2018) 699.
- [48] S. V. Gnedenkov, Y.P. Sharkeev, S.L. Sinebryukhov, V.S. Egorin, O.A. Khrisanfova, E. V. Legostaeva, A.G. Zavidnaya, A. V. Puz, I.A. Khlusov, and D.P. Opra, *Mater. Technol.* 31 (2016) 203.
- [49] T.S.N. Sankara Narayanan, I.S. Park, and M.H. Lee, *Prog. Mater. Sci.* 60 (2014) 1.
- [50] G. Wu, J.M. Ibrahim, and P.K. Chu, *Surf. Coatings Technol.* 233 (2013) 2.
- [51] G. Barati Darband, M. Aliofkhaezrai, P. Hamghalam, and N. Valizade, *J. Magnes. Alloy.* 5 (2017) 74.
- [52] A. Fattah-alhosseini, and M. Sabaghi Joni, *J. Mater. Eng. Perform.* 24 (2015) 3444.

- [53] R. Chaharmahali, K. Babaei, and A. Fattah-alhosseini, *Anal. Bioanal. Electrochem.* 11 (2019) 703.
- [54] C. Blawert, W. Dietzel, E. Ghali, and G. Song, *Adv. Eng. Mater.* 8 (2006) 511.
- [55] A. Keyvani, M. Zamani, A. Fattah-alhosseini, S.H. Nourbakhsh, and M. Bahamirian, *Mater. Res. Express.* 5 (2018) 086510.
- [56] R. Chaharmahali, M. Shadabi, K. Babaei, S.O. Gashti, and A. Fattah-alhosseini, *Anal. Bioanal. Electrochem.* 11 (2019) 38.
- [57] R. Chaharmahali, A. Fattah-alhosseini, and H. Esfahani, *J. Asian Ceram. Soc.* 8 (2020) 39.
- [58] W. Xue, Q. Zhu, Q. Jin, and M. Hua, *Mater. Chem. Phys.* 120 (2010) 656.
- [59] M. Sandhyarani, N. Rameshbabu, K. Venkateswarlu, D. Sreekanth, and C. Subrahmanyam, *J. Alloys Compd.* 553 (2013) 324.
- [60] M. Sandhyarani, N. Rameshbabu, K. Venkateswarlu, and L. Rama Krishna, *Surf. Coatings Technol.* 238 (2014) 58.
- [61] M. Sandhyarani, T. Prasada Rao, and N. Rameshbabu, *Appl. Surf. Sci.* 317 (2014) 198.
- [62] A.V. V. Apelfeld, A.M.M. Borisov, B.L.L. Krit, V.B.B. Ludin, M.N.N. Polyansky, E.A.A. Romanovsky, S.V. V. Savushkina, I.V. V. Suminov, N.V. V. Tkachenko, A.V. V. Vinogradov, and V.G.G. Vostrikov, *Surf. Coatings Technol.* 269 (2015) 279.
- [63] S.-F.F. Lu, B.-S.S. Lou, Y.-C.C. Yang, P.-S.S. Wu, R.-J.J. Chung, and J.-W.W. Lee, *Thin Solid Films.* 596 (2015) 87.
- [64] S. Cengiz, A. Uzunoglu, L. Stanciu, M. Tarakci, and Y. Gencer, *Surf. Coatings Technol.* 301 (2016) 74.
- [65] A.V. V. Apelfeld, A.A.A. Ashmarin, A.M.M. Borisov, A.V. V. Vinogradov, S.V. V. Savushkina, and E.A.A. Shmytkova, *Surf. Coatings Technol.* 328 (2017) 513.
- [66] S.L. Aktuğ, S. Durdu, E. Yalçın, K. Çavuşoğlu, and M. Usta, *Surf. Coatings Technol.* 324 (2017) 129.
- [67] S. Cengiz, Y. Azakli, M. Tarakci, L. Stanciu, and Y. Gencer, *Mater. Sci. Eng. C.* 77 (2017) 374.
- [68] M. Sowa, A. Kazek-Kęsik, A. Krzakała, R.P. Socha, G. Dercz, J. Michalska, and W. Simka, *J. Solid State Electrochem.* 18 (2014) 3129.
- [69] V.S. Rudnev, D.L. Boguta, T.P. Yarovaya, and P.M. Nedozorov, *Prot. Met. Phys. Chem. Surfaces.* 50 (2014) 360.
- [70] S. Aliasghari, P. Skeldon, X. Zhou, R. Valizadeh, T. Junginger, G.B.G.G. Stenning, and G. Burt, *J. Appl. Electrochem.* 49 (2019) 979.
- [71] Y. Ge, Y. Wang, Y. Cui, Y. Zou, L. Guo, J. Ouyang, D. Jia, and Y. Zhou, *Appl. Surf. Sci.* 491 (2019) 526.
- [72] S. Aliasghari, P. Skeldon, X. Zhou, R. Valizadeh, T. Junginger, G.B.G. Stenning, and G. Burt, *ECS J. Solid State Sci. Technol.* 8 (2019) N39.

- [73] S. Stojadinović, N. Tadić, N. Radić, P. Stefanov, B. Grbić, and R. Vasilić, *Appl. Surf. Sci.* 355 (2015) 912.
- [74] M. Sowa, J. Worek, G. Dercz, D.M. Korotin, A.I. Kukharenko, E.Z. Kurmaev, S.O. Cholakh, M. Basiaga, and W. Simka, *Electrochim. Acta.* 198 (2016) 91.
- [75] S. Stojadinović, and R. Vasilić, *J. Alloys Compd.* 685 (2016) 881.
- [76] Y.L. Ge, Y.M. Wang, Y.F. Zhang, L.X. Guo, D.C. Jia, J.H. Ouyang, and Y. Zhou, *Surf. Coatings Technol.* 309 (2017) 880.
- [77] B.L. Pereira, C.M. Lepienski, I. Mazzaro, and N.K. Kuromoto, *Mater. Sci. Eng. C.* 77 (2017) 1235.
- [78] M. Sowa, and W. Simka, *Surf. Coatings Technol.* 344 (2018) 121.
- [79] B.L. Pereira, A.R. da Luz, C.M. Lepienski, I. Mazzaro, and N.K. Kuromoto, *J. Mech. Behav. Biomed. Mater.* 77 (2018) 347.
- [80] Y. Ge, Y. Wang, J. Chen, Y. Zou, L. Guo, J. Ouyang, D. Jia, and Y. Zhou, *J. Alloys Compd.* 767 (2018) 7.
- [81] S. Stojadinović, J. Jovović, M. Petković, R. Vasilić, and N. Konjević, *Surf. Coatings Technol.* 205 (2011) 5406.
- [82] M. Petković, S. Stojadinović, R. Vasilić, and L. Zeković, *Appl. Surf. Sci.* 257 (2011) 10590.
- [83] M. Sowa, A. Kazek-Kęsik, R.P. Socha, G. Dercz, J. Michalska, and W. Simka, *Electrochim. Acta.* 114 (2013) 627.
- [84] C. Wang, F. Wang, and Y. Han, *Surf. Coatings Technol.* 214 (2013) 110.
- [85] H. Gao, Y.F. Jie, Z.Q. Wang, H. Wan, L. Gong, R.C. Lu, Y.K. Xue, D. Li, H.Y. Wang, L.N. Hao, and Y.Z. Zhang, *J. Mater. Chem. B.* 2 (2014) 1216.
- [86] K. Rokosz, T. Hryniewicz, P. Chapon, S. Raaen, and H. Ricardo Zschommler Sandim, *J. Spectrosc.* 2016 (2016) 1.
- [87] M.A.P.C. Goularte, G.F. Barbosa, N.C. da Cruz, and L.M. Hirakata, *Int. J. Implant Dent.* 2 (2016) 12.
- [88] C. Wang, F. Wang, and Y. Han, *Appl. Surf. Sci.* 361 (2016) 190.
- [89] Q.M. Zhao, G.Z. Li, H.L. Yang, and X.F. Gu, *Mater. Technol.* 32 (2017) 90.
- [90] M. Sowa, M. Woszczak, A. Kazek-Kęsik, G. Dercz, D.M. Korotin, I.S. Zhidkov, E.Z. Kurmaev, S.O. Cholakh, M. Basiaga, and W. Simka, *Appl. Surf. Sci.* 407 (2017) 52.
- [91] M. Sowa, and W. Simka, *Materials.* 11 (2018) 454.
- [92] R.F. Antonio, E.C. Rangel, B.A. Mas, E.A.R. Duek, and N.C. Cruz, *Surf. Coatings Technol.* 357 (2019) 698.
- [93] X. He, X. Zhang, X. Wang, and L. Qin, *Coatings.* 7 (2017) 45.
- [94] W. Yuan, B. Li, D. Chen, D. Zhu, Y. Han, and Y. Zheng, *ACS Biomater. Sci. Eng.* 5 (2019) 487.
- [95] L. Zhang, J. Zhang, C. Chen, and Y. Gu, *Corros. Sci.* 91 (2015) 7.

- [96] X. Lin, L. Tan, Q. Zhang, K. Yang, Z. Hu, J. Qiu, and Y. Cai, *Acta Biomater.* 9 (2013) 8631.
- [97] S.F.F. Fischerauer, T. Kraus, X. Wu, S. Tangl, E. Sorantin, A.C.C. Hänzi, J.F.F. Löffler, P.J.J. Uggowitzer, and A.M.M. Weinberg, *Acta Biomater.* 9 (2013) 5411.
- [98] Y. Wang, J. Wang, J. Zhang, and Z. Zhang, *Mater. Corros.* 56 (2005) 88.
- [99] S. Durdu, and M. Usta, *Appl. Surf. Sci.* 261 (2012) 774.
- [100] W. Xue, Z. Deng, R. Chen, and T. Zhang, *Thin Solid Films.* 372 (2000) 114.
- [101] J. Jiang, Q. Zhou, J. Yu, A. Ma, D. Song, F. Lu, L. Zhang, D. Yang, and J. Chen, *Surf. Coatings Technol.* 216 (2013) 259.
- [102] V.S. Rudnev, M.A. Medkov, T.P. Yarovaya, N.I. Steblevskaya, P.M. Nedovzorov, and M. V. Belobeletskaya, *Russ. J. Appl. Chem.* 85 (2012) 621.
- [103] A. Fattah-alhosseini, K. Babaei, and M. Molaei, *Surfaces and Interfaces.* 18 (2020) 100441.